Macromolecules

pubs.acs.org/Macromolecules Article

Dynamics of Bottlebrush Polymers in Solution by Neutron Spin Echo Spectroscopy

Karin J. Bichler,* Bruno Jakobi, Dirk Honecker, Laura R. Stingaciu, Thomas K. Weldeghiorghis, James H. P. Collins, and Gerald J. Schneider*

Cite This: *Macromolecules* 2022, 55, 9810–9819 Read Online

ACCESS | Metrics & More | Article Recommendations

ABSTRACT: We present dynamical and morphological studies on poly(dimethylsiloxane) (PDMS)-based bottlebrush polymers in solution. A combination of small-angle neutron scattering (SANS), pulsed field gradient nuclear magnetic resonance (PFG NMR), and neutron spin echo (NSE) spectroscopy was used to identify structural changes inherent in changing the side-chain length while keeping the backbone constant. These morphological changes are mirrored in the diffusion coefficient determined by PFG NMR, resulting in two coefficients for the elongated and one for the more spherical sample. Faster motions are tracked by NSE using the advantage of time- and length-scale resolutions with the diffusion coefficient predetermined by PFG NMR. Hereby, the sample with short side chains relaxes like wormlike micelles considering the longitudinal direction, whereas the dynamics along the radial extension shows a much stronger Q-dependence as known from any theory. The dynamical behavior within the blob region, covered with the more spherical sample, follows the predictions of Zimm as well as of Zilman and Granek (ZG).

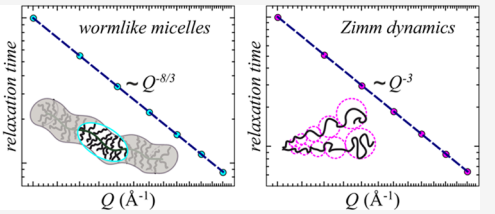

INTRODUCTION

Bottlebrush polymers have attracted great interest in recent times, regarding their morphology, dynamics, and their link to the outstanding properties compared to well-known linear polymers.[1−5] The extraordinary material behavior results from linear side chains densely grafted onto a linear backbone. Changing the length ratio of backbone to side chain enables different shapes, ranging from elongated to spherical objects.[2,6−8] Hereby, elongated bottlebrush polymers are seen as wormlike chains and spherical shapes are seen as star polymers.[1,9]

Most of the current work focuses on the morphology and the influence of parameters like solvent quality or other external stimuli on the conformation.[8,10−13] Comparatively few studies of the dynamics exist, mostly rheology, dielectric spectroscopy, fast field cycling NMR, or quasi-elastic neutron scattering (QENS).[2,3,14−18] Previous QENS studies on bottlebrushes showed a length-scale-dependent segmental relaxation within the side chains and a methyl group rotation confined to a threefold rotational jump. QENS is limited to fast relaxations in the time scale of $t \sim 0.001-1$ ns and small length scales of $d \sim 16-3$ Å corresponding to momentum transfers of $Q \sim 0.4-1.8$ Å^{-1}. To extend dynamical studies for longer times, up to $t \sim 100$ ns, and larger length scales $d \sim 42-157$ Å, neutron spin echo (NSE) spectroscopy is useful, especially for large-scale chain dynamics. This provides an overview of the dynamics of the entire bottlebrush polymer.

Here, we concentrate on the dynamics of bottlebrushes in solution by NSE with diffusion coefficients determined by pulsed field gradient nuclear magnetic resonance (PFG NMR). The morphological transition in our samples induced by changing the side-chain length while keeping the backbone constant has been investigated by small-angle neutron scattering (SANS). The essential information obtained is an elongated shape for the sample having a side-chain molecular weight of $M_n^{\text{side chain}} = 1800$ g/mol, while increasing $M_n^{\text{side chain}}$ to 11,500 g/mol results in more spherical objects. These different structural features of our samples are also resembled in the diffusion coefficient, as we either detect two or one coefficient, attributed to translational and rotational diffusion, depending on the morphology of our bottlebrush polymer. This overview indicates that there are different structural levels that may manifest in different microscopic dynamics. Considering the limited Q-window of NSE, characterizing the different structural levels is challenging. We take advantage of studying two samples with different side-chain molecular weights, which allows moving the dynamical features through the accessible Q-window of the NSE experiment. By that means, we can access the dynamical behavior along the longitudinal and the radial extension of the sample, as well as the dynamics within the side chains, i.e., within the blob region.

Received: June 6, 2022
Revised: September 21, 2022
Published: October 17, 2022

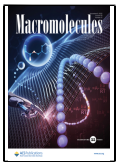

https://doi.org/10.1021/acs.macromol.2c01177
Macromolecules 2022, 55, 9810−9819

Hereby, the motions are compatible with the prediction of Zilman and Granek (ZG) for wormlike micelles in the case of the longitudinal extension, whereas the dynamics in the blob region follows Zimm as well as ZG for spherical micelles.[19−23] However, the region of radial extension shows a much stronger Q-dependence of the relaxation time and is attributed to a transition region.

Both samples together allow us to capture a complementary picture of the dynamics in bottlebrush polymers in different structural parts, achieved by "shifting" the structure through the available Q-window of NSE.

EXPERIMENTAL SECTION

Materials. For the present study, two PDMS-*g*-PDMS bottlebrush polymers in deuterated toluene have been investigated by small-angle neutron scattering (SANS), neutron spin echo (NSE) spectroscopy, and pulsed field gradient (PFG) NMR. The synthesis of both samples is based on anionic polymerization. Details can be found in Jakobi et al.[2] As illustrated in Table 1, the side-chain molecular weight, $M_n^{\text{side chain}}$, of both samples is different while M_n^{backbone} is kept constant. This implies a change in the ratios of the backbone to side-chain molecular weight, which results in a shape transition, confirmed by previous SANS experiments in deuterated cyclohexane.[2]

Table 1. Number Average Molecular Weight, M_n, Polydispersity Index, PDI, and Grafting Density, $[z^*]$, of the Two Bottlebrush Polymers and Single Component, i.e., Single Side Chain and Single Backbone before the Grafting Reaction[2]

	single linear chain M_n (g/mol) (PDI)	(PDI) bottlebrush M_n(kg/mol) (PDI) $[z^*]$
side chain I	1800 (1.2)	157 (1.1) [30]
side chain II	11,500 (1.1)	1106 (1.2) [41]
backbone	13,500 (1.2)	

Two concentrations have been measured with SANS: the low concentration, Φ = 0.5 vol %, to obtain the form factor in *d*-toluene and the high concentration, Φ = 30 vol %, which is the same concentration as that used for dynamical experiments to get information about the structural changes in the available Q-range at NSE.

Small-Angle Neutron Scattering (SANS). Small-angle neutron scattering (SANS) delivers information about time-averaged structural arrangements and correlations between nanoscale objects in terms of the momentum transfer, $Q = 4\pi/\lambda \cdot \sin\left(\frac{\theta}{2}\right)$, depending on the scattering angle θ and the wavelength λ.[24] Deuterated and protonated species differ in scattering length densities, ρ, giving rise to a contrast $\Delta\rho$, resulting in a momentum transfer-dependent scattering intensity, $I(Q)$, comprising form factor, $P(Q)$, and structure factor, $S(Q)$

$$I(Q) \propto P(Q) \cdot S(Q) \tag{1}$$

While $P(Q)$ accounts for the structural information, $S(Q)$ gives information about the correlations. Usually, at low concentrations of the polymer in the solvent, the scattering curve can be described by the form factor. By increasing the concentration, the objects are getting closer to each other, resulting in a notable contribution from the structure factor.[25] Using appropriate model functions gives information about the geometry (shape, size and distribution, and composition profile) of the scattering objects. The examined PDMS-*g*-PDMS bottlebrush polymers at a low concentration in solution can be well described by the form factor of a semiflexible polymer chain, including the blob contribution for the high Q-region, as reported previously.[2]

Small-angle neutron scattering (SANS) measurements over a wavelength range of λ = (0.9−13.5) Å have been performed at the time-of-flight beamline LAMOR located at the pulsed neutron source ISIS, Didcot, United Kingdom. Samples were filled in circular quartz cells with a path length of d = 1 mm at room temperature. The data were masked, toluene background-corrected, radially averaged, and scaled to absolute units.

Neutron Spin Echo (NSE) Spectroscopy. Neutron spin echo (NSE) spectroscopy measures the coherent and incoherent intermediate scattering functions $S_{coh}(Q, t)$ and $S_{inc}(Q, t)$ of the polymer system

$$S_{coh}(Q, t) \propto \langle R_i(t) - R_j(0) \rangle$$
$$S_{inc}(Q, t) \propto \langle R_i(t) - R_i(0) \rangle \tag{2}$$

with the positions i and j within the polymer chain.[25,26] Depending on the sample composition in regard to protonated and deuterated, the coherent and incoherent scattering contributions can be enhanced. While a fully protonated system has a large incoherent scattering cross section, the obtained scattering signal is dominated by the incoherent intermediate scattering function, describing self-diffusional processes.

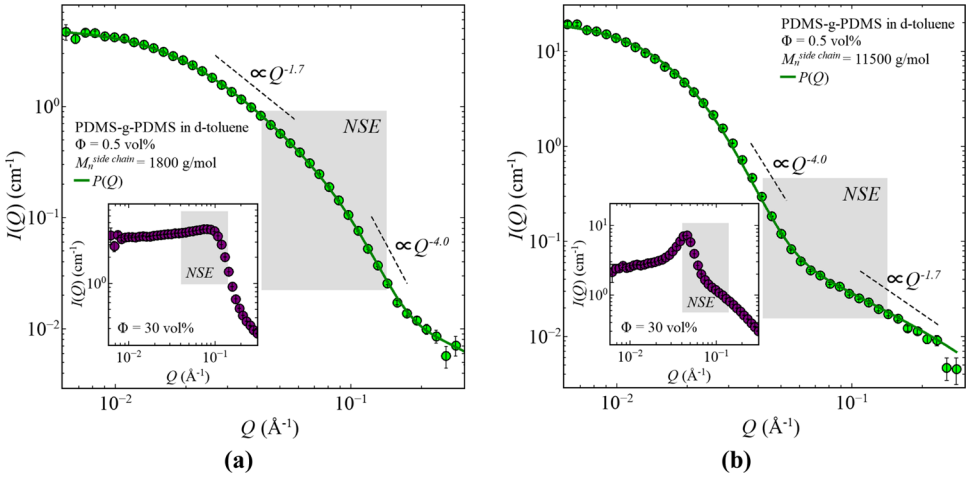

Figure 1. Scattering intensity, $I(Q)$, as a function of momentum transfer, Q, for the PDMS-*g*-PDMS bottlebrush samples investigated in *d*-toluene. (a) Low concentration, Φ = 0.5 vol %, of PDMS-*g*-PDMS bottlebrush with $M_n^{\text{side chain}}$ = 1800 g/mol. (b) Low concentration, Φ = 0.5 vol %, of PDMS-*g*-PDMS bottlebrush with $M_n^{\text{side chain}}$ = 11,500 g/mol. Insets: high concentrations, Φ = 30 vol %, of the respective PDMS-*g*-PDMS. Gray-shaded areas indicate the measured Q-region at NSE. Dashed lines represent the proportionality to power laws.

https://doi.org/10.1021/acs.macromol.2c01177
Macromolecules 2022, 55, 9810−9819

In contrast, mixtures comprising deuterated and protonated species are dominated by the coherent intermediate scattering function. Our sample systems contain Φ = 30 vol % protonated polymer in the deuterated solvent; thus, we get information about the coherent intermediate scattering function $S_{coh}(Q, t)$.[27] This correlation function is also known as a pair correlation function, describing the time evolution of two polymer chains with respect to each other, known as large-scale polymer dynamics, $S_{chain}(Q, t)$.[26]

Often, the scattering data comprises different dynamical parts. The most common in NSE experiments is the combination of diffusion and large-scale polymer dynamics, which can be described in the easiest way by a diffusion part together with the stretched exponential function

$$\frac{S(Q,t)}{S(Q)} = \exp(-Q^2Dt)\cdot\exp\left(-\left(\frac{t}{\tau(Q)}\right)^{\beta(Q)}\right) \quad (3)$$

including diffusion coefficient, D, relaxation time, $\tau(Q)$, and stretching parameter, $\beta(Q)$. In our case, the diffusion coefficients have been predetermined by pulsed field gradient NMR and fixed to the resulting values, leading to a reduced number of fitting parameters. All of the data has been normalized that $\lim_{t\to 0}\frac{S(Q,t)}{S(Q)} = 1$. This allows us to avoid a Q-dependent scaling factor.

In the case of Q-dependent stretching parameters, the relaxation time can be transferred into the average relaxation time, $\langle\tau\rangle$, using $\langle\tau\rangle = \frac{\tau(Q)}{\beta(Q)}\cdot\Gamma\left(\frac{1}{\beta(Q)}\right)$.[26] Furthermore, for scattering data taken at a high sample concentration (ϕ = 30 vol %), as presented here, the inter-bottlebrush interaction comes into play in the available Q-range (Figure 1a). This influences the relaxation time, which needs to be corrected by the division of the structure factor $S(Q)$.[28,29] The resulting intrinsic relaxation time

$$\langle\tau\rangle_{int} = \langle\tau\rangle\cdot\frac{1}{S(Q)} \quad (4)$$

has no contributions from the correlation of neighboring bottlebrush polymers. This is also known as the de-Gennes narrowing.[28,29]

Neutron spin echo experiments at room temperature (T = 298 K) were conducted using the neutron spin echo spectrometer at SNS, SNS−NSE, BL-15, at the Spallation Neutron Source of the Oak Ridge National Laboratory, Oak Ridge, TN.[30] Hereby, configurations with wavelengths λ = 8 and 11 Å^{-1} were used to access a Q-range of 0.035−0.15 Å^{-1} and a Fourier time range of t = (0.03−130) ns. For the measurements, the different polymer solutions of Φ = 30 vol % dissolved in d-toluene were filled in aluminum top loader sample cells with a thickness of d = 1 mm. Deuterated toluene was measured separately as a solvent and used for background subtraction during data reduction.

Pulsed Field Gradient (PFG) NMR. The diffusion coefficient was determined separately by pulsed field gradient (PFG) NMR measurements at the same samples and same temperatures. Hereby, the self-correlation function of the protonated part in the sample is measured, similar to incoherent neutron spectroscopy experiments. In PFG NMR, the diffusion coefficient is extracted from the field gradient pulse, q, dependent on the spin echo decay $A(q^2)$, with $q = \gamma_H\delta g$ including the proton gyromagnetic ratio, γ_H, gradient pulse length, δ, and the strength of the field gradient pulse, g, whereby Δ denotes the observation time between two gradient pulses

$$\frac{A(q^2)}{A(0)} = \exp\left(-q^2D\left(\Delta - \frac{\delta}{3}\right)\right) \quad (5)$$

Representing $A(q^2)$ vs q^2, the diffusion coefficient, D, can be determined as the slope of the data points.[31,32]

Pulsed field gradient (PFG) NMR measurements were performed at the AMRIS facility using a Bruker AVIII 600 MHz magnet, equipped with a Bruker DIFF30 probe and an EVT 5 mm ^{1}H coil. Data for this publication was acquired with a fully convection compensated spin echo-based sequence,[33] with an equivalent δ = 2.0 ms and Δ = 100 ms. Sixteen different gradient strengths were used, linearly spaced to a maximum value of 1500 G/cm. Sine-shaped gradient pulses of length (3.14 ms, equivalent to a 2 ms square pulse) were used to minimize eddy currents. A total repetition time of 8 s was used. Based on T_1 measurements using an inversion recovery sequence, this was equivalent to 4 × T_1. The sample temperature was 25 °C and had been previously calibrated using a MeOH standard. The samples were stored at room temperature prior to the NMR experiments and further allowed to equilibrate for 30 min with the spectrometer prior to data acquisition.

RESULTS AND DISCUSSION

Small-Angle Neutron Scattering. Small-angle neutron scattering on a low concentration, Φ = 0.5 vol %, results in the form factor, $P(Q)$, of our PDMS-g-PDMS bottlebrush polymers in d-toluene, as shown in Figure 1.

The scattering curve for the bottlebrush polymer with $M_n^{\text{side chain}}$ = 1800 g/mol (Figure 1a) shows two kinks, connected to the overall length, L ($Q \sim 0.01$ Å^{-1}), and to the side-chain length, i.e., the radius, R, of the bottlebrush polymer ($Q \sim 0.08$ Å^{-1}). The intensity in the intermediate Q-region shows a power law dependence of $I(Q) \propto Q^{-d_f}$ with d_f = 1.7, suggesting an elongated shape in a good solvent, with Flory exponent $\nu = \frac{1}{d_f} = 0.588$.[2,34] This number is compatible with our chosen solvent, deuterated toluene.[35] Continuing to higher Q-values, the so-called blob region emerges.[34] In this region, the polymer chain behaves as an unperturbed chain forming a Gaussian coil.[36] Increasing the side-chain length to $M_n^{\text{side chain}}$ = 11,500 g/mol (Figure 1b) with a constant backbone length shifts the second kink, i.e., the thickness-related feature, to lower Q-values. The blob region shifts toward lower Q-values indicative of an increased blob size. Both are compatible with the increasing radius, R, induced by longer side chains.

Since the structures resemble elongated, yet flexible shapes, both samples can be well described with the form factor based on a semiflexible polymer chain, accounting for the backbone and a star-like monomeric density profile, $\varphi(r)$, for considering the side chains.[34] The additional contribution from the internal side-chain structure is included in the blob contribution for the high Q-region. The total scattering function, $I(Q)$, for elongated bottlebrush polymers can be expressed as

$$I(Q) = \Phi V_{total}\Delta\rho^2\cdot\left(P_{SPC}(Q)\cdot P_{CS}(Q) + a\cdot\frac{P_{blob}(Q)}{1+\nu_{EV}P_{blob}(Q)}\right) \quad (6)$$

with concentration, Φ, contrast, $\Delta\rho$, scaling parameter, a, and total volume, V_{total}, of the bottlebrush polymer, including backbone and all side chains. Hereby, $P_{SPC}(Q)$, $P_{CS}(Q)$, and $P_{blob}(Q)$ describe the form factor of a semiflexible polymer chain, the cross section, and the blob contribution, respectively. The analysis is done in the same way as previously published, and details on the procedure are described in Jakobi et al.[2]

The resulting fit parameters for describing both low-concentration samples are summarized in Table 2.

Comparing the current fitting values with that of a previous study,[2] both results are well compatible despite the different solvents, i.e., d-cyclohexane vs d-toluene. Since both solvents

https://doi.org/10.1021/acs.macromol.2c01177
Macromolecules 2022, 55, 9810−9819

Table 2. Length, L, Radius, R, Kuhn Length, l_k, and Blob Size, ξ, of the Two Samples Investigated[a]

	PDMS-g-PDMS $M_n^{\text{side chain}}$ = 1800 g/mol	PDMS-g-PDMS $M_n^{\text{side chain}}$ = 11,500 g/mol
length L (Å)	795	842
radius R (Å)	8.7	46.7
Kuhn length l_k (Å)	41.0	43.0
blob size ξ (Å)	8.0	19.0

[a]Standard deviations are <1%.

are classified to be as good solvents for PDMS-based systems, this result is plausible.

Increasing the concentration from Φ = 0.5 to 30 vol % brings the bottlebrush polymers closer together, resulting in a well-pronounced contribution of the structure factor, $S(Q)$, as seen in the insets of Figure 1. Dividing the scattering intensity, $I(Q)$, by the form factor, $P(Q)$, results in good approximation of the structure factor, $S(Q) \sim I(Q)/P(Q)$, allowing an easier estimate of the distance, d, of the neighbored bottlebrush polymer by $d = \frac{2\pi}{Q_{max}}$ (Figure 2).

Comparing this distance with the radius of the respective bottlebrush polymer shows that none of the samples is above the overlap concentration at the investigated concentration, Φ = 30 vol %, for the NSE experiment.

As seen in the shaded areas in Figure 1, at the available Q-region of NSE, we do not reach the overall size of the bottlebrush polymers (Guinier plateau at low Q-values). While for the PDMS-g-PDMS with $M_n^{\text{side chain}}$ = 1800 g/mol we cover dynamics from the elongated shape as well as of the radial structure, for the PDMS-g-PDMS with $M_n^{\text{side chain}}$ = 11,500 g/mol we have a transition from the internal side-chain structure reaching the radial structure (Figure 3).

Pulsed Field Gradient NMR. For both samples, the diffusion coefficients were determined separately by PFG NMR and analyzed with eq 5 to extract the diffusion coefficient as the slope of the q-dependent normalized spin echo decay $A(q^2)/A(0)$ (Figure 4). In a further step, this reduces the number of fit parameters for the NSE analysis since the diffusion coefficient was fixed to the obtained values.

As seen in Figure 4a, for the sample having the shorter side chains, $M_n^{\text{side chain}}$ = 1800 g/mol, two different diffusion coefficients are detected, D_{fast} = 3.66 ×10^{-12} m^2/s and D_{slow} = 6.92 × 10^{-13} m^2/s, which seems to be connected with the elongated shape (Figure 1a). In contrast, the sample having the more spherical shape with $M_n^{\text{side chain}}$ = 11,500 g/mol (Figure 1b) shows only one diffusion coefficient, D_{fast} = 2.86 × 10^{-13} m^2/s, in the available range. However, this does not exclude the existence of a second slower diffusion process outside the available experimental range PFG NMR has access to.

Neutron Spin Echo Spectroscopy. Hereafter, we present the results of neutron spin echo (NSE) experiments and compare different approaches to describe $S(Q, t)/S(Q)$ appropriately. The diffusion coefficient was taken from the previous PFG NMR measurement and fixed to the determined values leading to a reduced number of fitting parameters.

Neutron Spin Echo on PDMS-g-PDMS with $M_n^{\text{side chain}}$ = 1800 g/mol. Experimental results of PDMS-g-PDMS with $M_n^{\text{side chain}}$ = 1800 g/mol, ϕ = 30%, are presented in Figure 5. Data analysis has been done with the following equation

$$\frac{S(Q,t)}{S(Q)} = \exp(-Q^2 D_{fast} t)\cdot\exp(-Q^2 D_{slow} t)\cdot \exp\left(-\left(\frac{t}{\tau(Q)}\right)^{\beta(Q)}\right) \quad (7)$$

incorporating both diffusion coefficients, D_{fast} and D_{slow} (Figure 5a). This approach results in the Q-dependent relaxation time, $\tau(Q)$, and stretching parameter, $\beta(Q)$ (Figure 5b).

The obtained relaxation time has been transferred into the average relaxation time, $\langle\tau\rangle$, and furthermore by considering the de-Gennes narrowing (eq 4) into the intrinsic relaxation time, $\langle\tau\rangle_{int}$. This was needed due to the high sample concentration.[28,29]

As seen in Figure 6, two power law regions evolve, with different Q-dependencies. While the lower Q-values show a behavior proportional to $Q^{-2.4}$, the high Q-region falls off with $Q^{-4.7}$ with the transition point located at Q = 0.09 $Å^{-1}$.

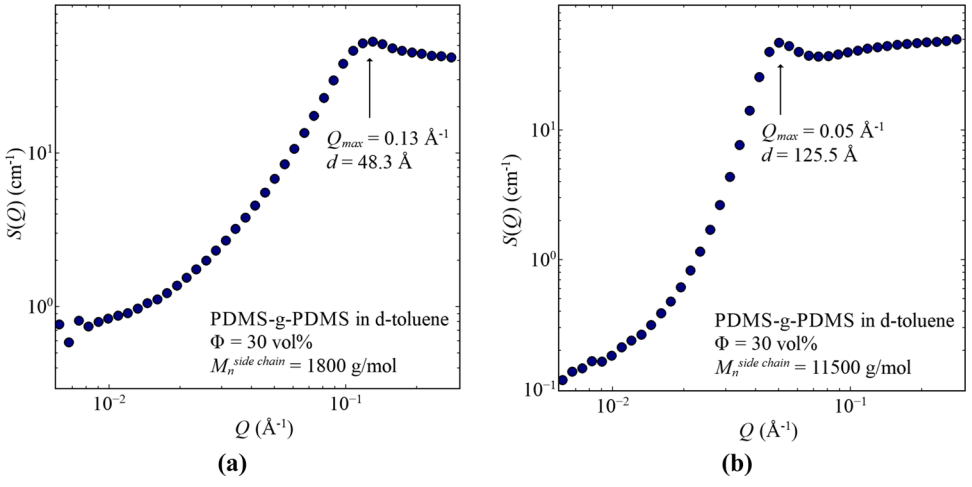

Figure 2. Structure factor, S(Q), as a function of momentum transfer, Q, for the PDMS-g-PDMS bottlebrush samples in d-toluene. (a) High concentration, Φ = 30 vol %, of PDMS-g-PDMS bottlebrush with $M_n^{\text{side chain}}$ = 1800 g/mol. (b) High concentration, Φ = 30 vol %, of PDMS-g-PDMS bottlebrush with $M_n^{\text{side chain}}$ = 11,500 g/mol. Arrows emphasize the peak position.

https://doi.org/10.1021/acs.macromol.2c01177
Macromolecules 2022, 55, 9810−9819

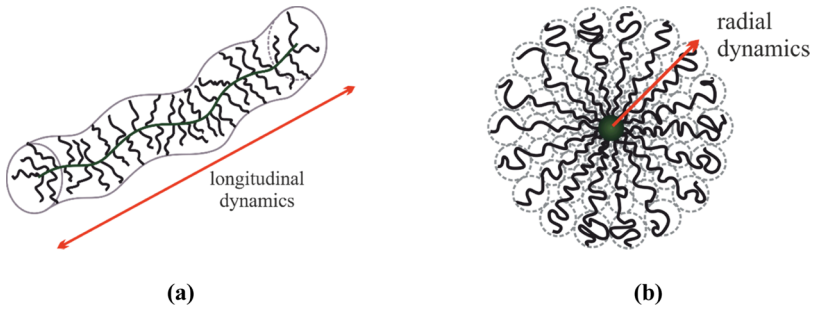

Figure 3. Simplified illustration of the longitudinal (a) and radial (b) dynamics.

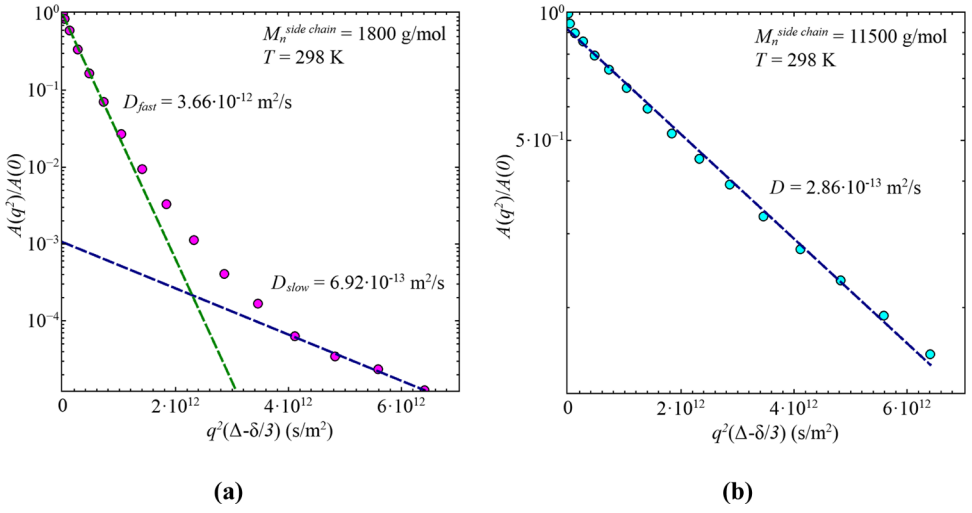

Figure 4. Normalized spin echo decay $A(q^2)/A(0)$ as a function of $q^2(\Delta - \delta/3)$ at T = 298 K for PDMS-*g*-PDMS in *d*-toluene with (a) $M_n^{side\ chain}$ = 1800 g/mol and (b) $M_n^{side\ chain}$ = 11,500 g/mol. Lines are a description with eq 4.

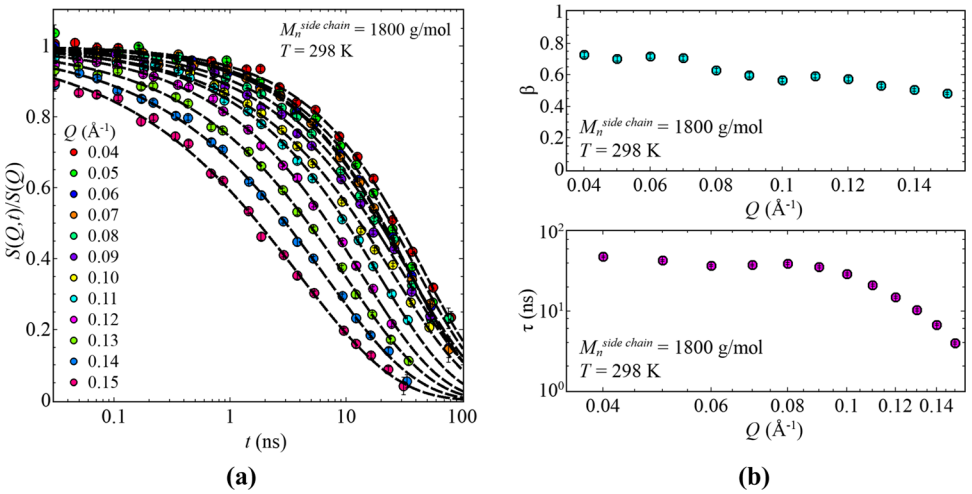

Figure 5. (a) Scattering function, $S(Q, t)/S(Q)$, as a function of time, t, for PDMS-*g*-PDMS with $M_n^{side\ chain}$ = 1800 g/mol with ϕ = 30 vol % in *d*-toluene at T = 298 K for different Q-values, as indicated. The dashed line represents the description with eq 7. (b) Stretching parameter, β, and relaxation time, τ, as a function of momentum transfer, Q, for PDMS-*g*-PDMS with $M_n^{side\ chain}$ = 1800 g/mol with ϕ = 30 vol % in *d*-toluene at T = 298 K.

This initial analysis of the intermediate scattering function points to two separate regions, with each range having the same Q-independent stretching parameter, β. A comparison with the static structure factor indicates a possible splitting into three different regions with different stretching parameters (Figure 7).

Hereby, regions I and III have been treated with constant stretching parameters, whereas the transition region asks for Q-dependent β values. This approach describes the scattering data in a good way, as seen in Figure 8. The different line styles—dashed (region I) vs dotted (region III)—indicate the different regions illustrated in Figure 7.

https://doi.org/10.1021/acs.macromol.2c01177
Macromolecules 2022, 55, 9810−9819

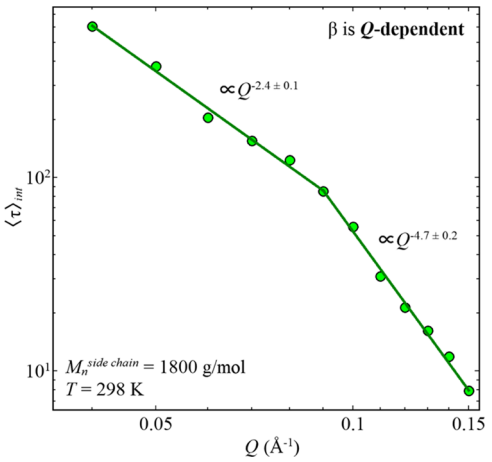

Figure 6. Intrinsic relaxation time, $\langle\tau\rangle_{int}$, as a function of momentum transfer, Q, for PDMS-*g*-PDMS with $M_n^{side\ chain}$ = 1800 g/mol with ϕ = 30 vol % in *d*-toluene at T = 298 K, obtained by fitting $S(Q, t)/S(Q)$ with stretching parameter, β, taken as Q-dependent. Solid lines represent the description of power laws. Error bars are within the symbol size and omitted.

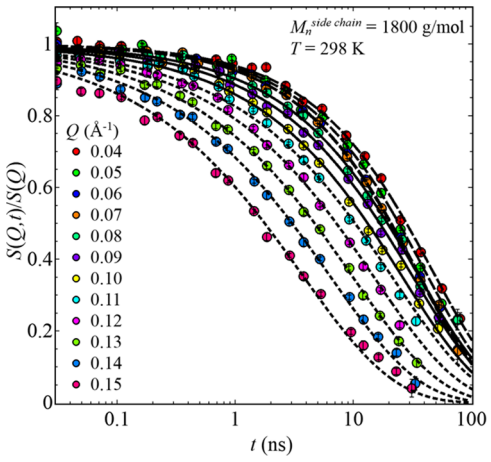

Figure 8. Normalized scattering function, $S(Q, t)/S(Q)$, as a function of time, t, for PDMS-*g*-PDMS with $M_n^{side\ chain}$ = 1800 g/mol with ϕ = 30 vol % in *d*-toluene at T = 298 K for different Q-values, as indicated. The different styled lines (dashed vs dotted) indicate region I and region III, fitted with eq 7 with shared stretching parameters, β. Solid lines indicate region II, fitted with eq 7 having independent β values.

The resulting stretching parameters, β, are illustrated in Figure 9, showing three regions, two with a constant β and a clear transition from β = 0.71 to 0.53, as introduced, while the intrinsic relaxation time, $\langle\tau\rangle_{int}$, shows two different power law regions. These regions remind us of the SANS data from the sample. Here, in the available Q-range, we cover two structural regions, i.e., along the longitudinal direction and in the radial direction (Figure 1a). Similar structural correlations can be attributed to the NSE data, i.e., dynamics along the longitudinal direction in the low Q-region, which changes into the radial direction at $Q \sim 0.09$ Å^{-1}. The transition point directly corresponds to the maximum of the scattering intensity at the high-volume concentration (Figure 7). Considering the two power laws, $\langle\tau\rangle_{int} \propto Q^{-2.5}$ in the Q-range attributed to the elongated part of the bottlebrush architecture, and $\langle\tau\rangle_{int} \propto Q^{-5.6}$ in the radial part of the bottlebrush, the dynamics changes substantially once the transition occurs.

The behavior at the low Q-values, i.e., the elongated structural region, is similar to those known for wormlike micelles.[19,20] In the framework of the theory by Zilman and Granek, the stretching parameter for wormlike micelles is predicted to be β_{ZG} = 3/4 resulting in a dependence of the relaxation rate on momentum transfer of $\tau \propto Q^{-8/3}$. Here, the stretching parameter is β = 0.71 close to the theoretical value; also, the relaxation time dependence with $\langle\tau\rangle_{int} \propto Q^{-2.5}$ is close to $\tau \propto Q^{-8/3}$. Therefore, the low Q-region in the presented sample is compatible with the dynamics of an elongated flexible object, i.e., with dynamics along the elongated shape of the bottlebrush polymer. Continuing to the higher Q-values that cover the radial extension of the bottlebrush polymer, the relaxation time is proportional to $Q^{-5.6}$ with a stretching parameter of β = 0.53. Intuitively, it makes sense to compare those values with spherical micelles or star polymers. However, for spherical micelles, it is predicted that β_{ZG} = 2/3 leading to a Q-dependence for the relaxation time of $\tau \propto Q^{-3}$.[20,21] Hence, the Q-dependence of the relaxation time of the bottlebrush polymer is much stronger than those known for any spherical systems. The reason for this unexpected behavior is unknown and deserves further inspection.

In summary, even if the dynamics at the larger length scales follows the relaxation behavior known from wormlike micelles, the relaxation in the radial region depends much stronger on

I. $Q = (0.04 - 0.07)$ Å^{-1}

II. Transition region
$Q = (0.08 - 0.10)$ Å^{-1}

III. $Q = (0.11 - 0.15)$ Å^{-1}

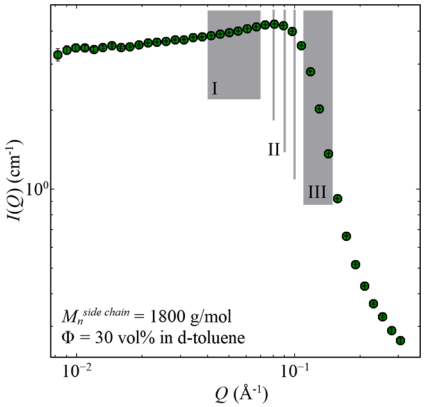

Figure 7. Scattering intensity, $I(Q)$, as a function of momentum transfer, Q, for PDMS-*g*-PDMS with $M_n^{side\ chain}$ = 1800 g/mol with ϕ = 30 vol % in *d*-toluene. Shaded areas indicate different regions.

https://doi.org/10.1021/acs.macromol.2c01177
Macromolecules 2022, 55, 9810−9819

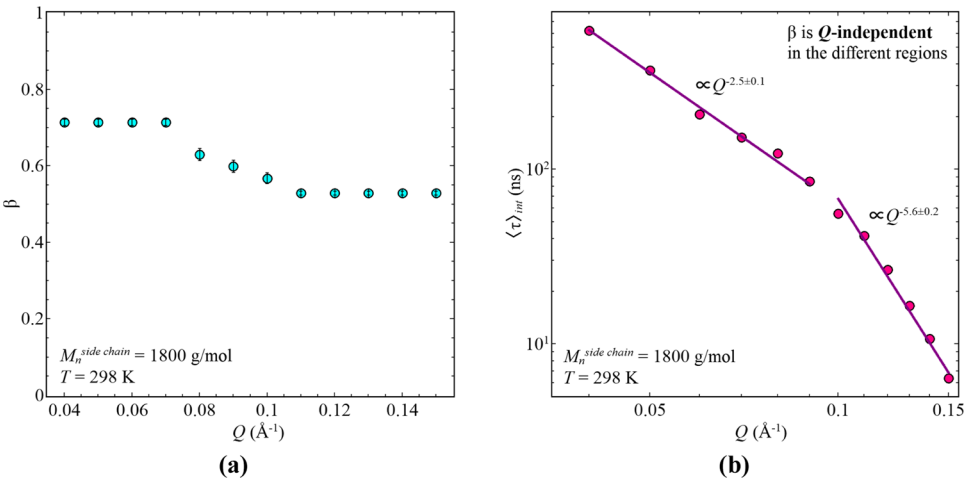

Figure 9. (a) Stretching parameter, β, as a function of momentum transfer, Q, for PDMS-g-PDMS with $M_n^{\text{side chain}}$ = 1800 g/mol with ϕ = 30 vol % in d-toluene at T = 298 K. (b) Intrinsic relaxation time, $\langle\tau\rangle_{\text{int}}$, as a function of momentum transfer, Q, for PDMS-g-PDMS with $M_n^{\text{side chain}}$ = 1800 g/mol with ϕ = 30 vol % in d-toluene at T = 298 K. Solid lines are the descriptions with power laws. Error bars are within the symbol size and omitted.

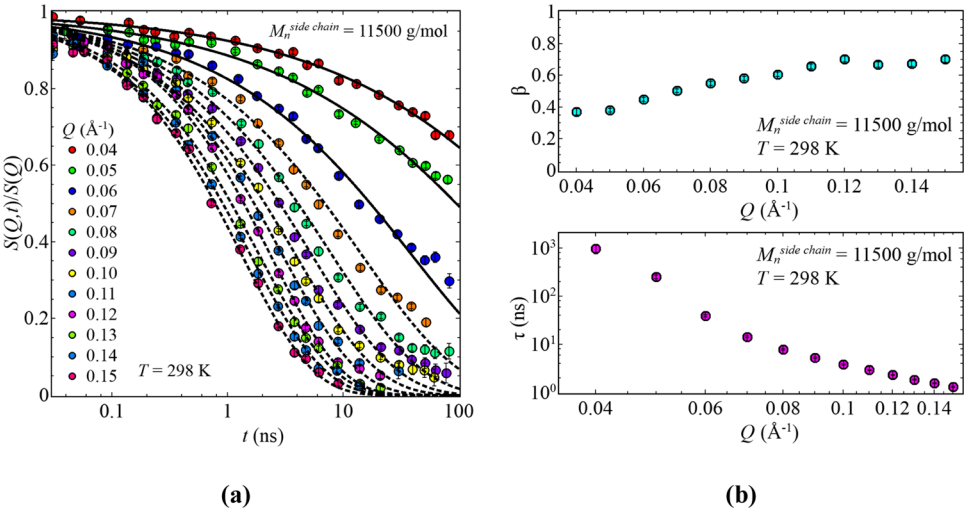

Figure 10. (a) Scattering function, $S(Q, t)/S(Q)$, as a function of time, t, for PDMS-g-PDMS with $M_n^{\text{side chain}}$ = 11,500 g/mol with ϕ = 30 vol % in d-toluene at T = 298 K for different Q-values, as indicated. The dashed line represents the description with eq 7 including one diffusion coefficient. (b) Stretching parameter, β, and relaxation time, τ, as a function of momentum transfer, Q, for PDMS-g-PDMS with $M_n^{\text{side chain}}$ = 11,500 g/mol with ϕ = 30 vol % in d-toluene at T = 298 K.

the surrounding environment and is strongly influenced on a small length scale compared to spherical micelles.

PDMS-*g*-PDMS with $M_n^{\text{side chain}}$ = 11,500 g/mol. The second sample of investigation has different structural features in the available Q-range, bringing us from the dynamics of the radial part to the dynamics of the blobs. As seen in Figure 1b, the Q-range of NSE covers both parts, but mainly the blob region, i.e., the dynamics within the side chains. This is also visible in the $S(Q, t)/S(Q)$ data since the dynamic structure factor at the lowest three Q-values Q = 0.04, 0.05, 0.06 Å^{-1} has different behavior compared to the other.

As a first approach, the same steps were taken as reported for the previous sample, whereby this time, one diffusion coefficient was incorporated into the fitting function. As seen in Figure 10, especially in the Q-dependence of the relaxation times (Figure 10b), we clearly have two different parts in the covered Q-region, I: Q = (0.04−0.06) Å^{-1} and II: Q = (0.07−0.15) Å^{-1}. Hereby, the low Q's, region I, can be well described by the explained procedure. However, in region II, the data seems to show a plateau at long times, instead of a full decay to zero.

The resulting power laws for the Q-dependence of the intrinsic relaxation time are $\langle\tau\rangle_{\text{int}} \propto Q^{-10.9}$ at low Q's (region I) and $\langle\tau\rangle_{\text{int}} \propto Q^{-3.9}$ at higher Q's (region II) (Figure 11). Such a strong dependence as seen in the low Q-region has not been reported so far. However, we need to be careful because a comparison with the SANS data (Figure 1b) illustrates that this huge exponent relates to a Q-range, which could be affected by the transition between two different regions. Hence, the rapid decrease could simply be a consequence of the existence of more than one single process. Therefore, for further analysis and interpretation, region I, Q = 0.04, 0.05, 0.06 Å^{-1}, will be excluded.

Continuing to the higher Q-values, the power law of $\langle\tau\rangle_{\text{int}} \propto Q^{-3.9}$ seems to be well developed. However, there are slight deviations at higher Fourier times owing to the emergence of a

https://doi.org/10.1021/acs.macromol.2c01177
Macromolecules 2022, 55, 9810−9819

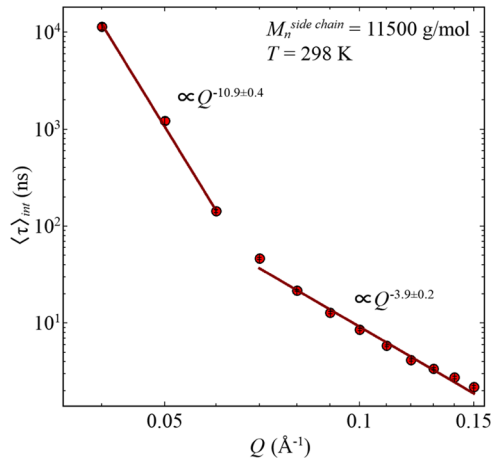

Figure 11. Intrinsic relaxation time, $\langle\tau\rangle_{int}$, as a function of momentum transfer, Q, for PDMS-g-PDMS with $M_n^{side\ chain}$ = 11,500 g/mol with ϕ = 30 vol % in d-toluene at T = 298 K. Solid lines are the descriptions with power laws. Error bars are within the symbol size and omitted.

plateau in the long-time limit (Figure 10a). Therefore, we analyze the data including geometrical constraints indicated by the plateau using the parameter $E(Q)$

$$\frac{S(Q,t)}{S(Q)} = E(Q) + (1 - E(Q))\cdot\exp(-Q^2Dt)\cdot \exp\left(-\left(\frac{t}{\tau(Q)}\right)^{\beta(Q)}\right) \quad (8)$$

Here, eq 4 has still been used for calculating $\langle\tau\rangle_{int}$, as done previously.

Using eq 8, a better description of the experimental data can be accomplished. The stretching parameter, β, has been treated as Q-dependent resulting in the range of β = 0.6−0.75 with an average of $\langle\beta\rangle$ = 0.67 (Figure 12).

The resulting Q-dependence of the average intrinsic relaxation time $\langle\tau\rangle_{int}$ shows a power law behavior of $\langle\tau\rangle_{int} \propto Q^{-2.8}$ (Figure 13a). This exponent is close to that of Zimm dynamics ($\tau \propto Q^{-3}$) and is also predicted by Zilman and Granek ($\tau \propto Q^{-3}$) for spherical micelles.

For many cases, relaxation in geometrical confinements can be well described by analytical models, like for diffusion within a sphere or cylinder.[37] In the case of our bottlebrush polymer, the geometrical confinement, $E(Q)$, does not follow any of those known models (Figure 13b).

Compared to the diffusion within a sphere, the values indicate less confinement at the Q-values of Q = 0.07−0.09 Å^{-1}, while stronger confinement at Q = 0.1−0.15 Å^{-1}. Similar results are for the comparison with a cylindrical confinement. Our tests indicate that the simple classical potentials cannot describe the experimental observations. One simple reason might be the small values, which could be indicative of dynamics almost entirely relaxed, with less influence of a specific geometrical constraint. However, it is also likely that the neighboring chains induce restrictions that might strongly depend on the distance to the backbone.

SUMMARY AND CONCLUSIONS

The presented results illustrate the first neutron spin echo experiments on bottlebrush polymer systems in solution, focusing on the normalized pair correlation function, which has access to large-scale polymer dynamics. For covering relaxations over a broad length scale with NSE, we have selected two different samples, which show different structural features in the available Q-range of the NSE experiment. While the first sample, having a more elongated shape, covers length scales along the elongated structural feature as well as the transition into the radial dimension, the second sample, with an expanded cross section, covers mostly the blob region, i.e., the internal side-chain region. Both together offer a broad picture of bottlebrush dynamics in solution spread over different parts of the bottlebrush itself. As determined by PFG NMR, the diffusion coefficients for both samples do not have a substantial influence on the dynamics in the time range of up to 100 ns but were included for data analysis of the neutron spin echo data.

In the more elongated sample having side chains of $M_n^{side\ chain}$ = 1800 g/mol, the dynamics of the longitudinal direction is well compatible with the dynamical behavior of wormlike

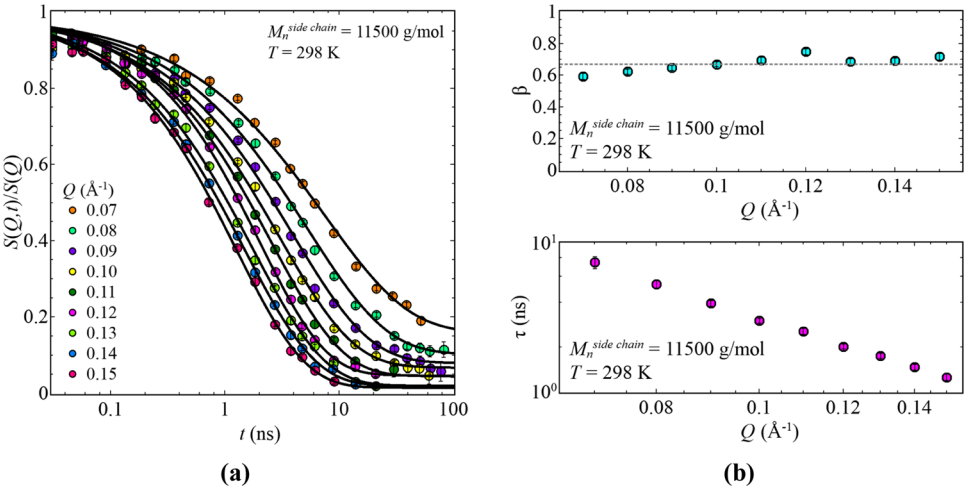

Figure 12. (a) Normalized scattering function, $S(Q,t)/S(Q)$, as a function of time, t, for PDMS-g-PDMS with $M_n^{side\ chain}$ = 11,500 g/mol with ϕ = 30 vol % in d-toluene at T = 298 K for different Q-values, as indicated. The lines represent fits with eq 8. (b) Stretching parameter, β, and relaxation time, τ, as a function of momentum transfer, Q, for PDMS-g-PDMS with $M_n^{side\ chain}$ = 11,500 g/mol with ϕ = 30 vol % in d-toluene at T = 298 K.

https://doi.org/10.1021/acs.macromol.2c01177
Macromolecules 2022, 55, 9810−9819

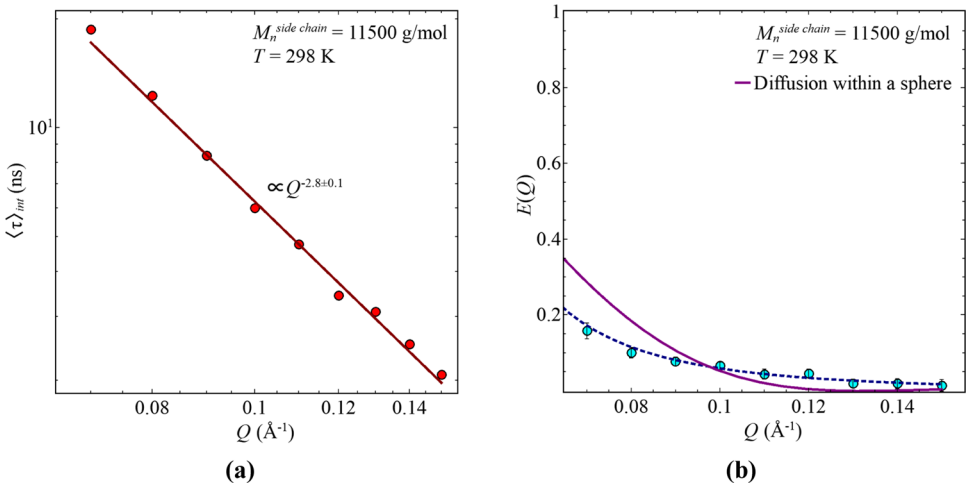

Figure 13. (a) Intrinsic relaxation time, $\langle\tau\rangle_{int}$, as a function of momentum transfer, Q, for PDMS-*g*-PDMS with $M_n^{side\ chain}$ = 11,500 g/mol with ϕ = 30 vol % in *d*-toluene at T = 298 K. The solid line is the description of power laws. Error bars are within the symbol size and omitted. (b) Geometrical confinement, $E(Q)$, as a function of momentum transfer, Q, for PDMS-*g*-PDMS with $M_n^{side\ chain}$ = 11,500 g/mol with ϕ = 30 vol % in *d*-toluene at T = 298 K. The dotted line is a guide for the eye. The solid line is the geometrical confinement for diffusion within a sphere.

micelles based on the stretching parameter, β = 0.71 ∼ 3/4, and on the Q-dependence of the relaxation time, $\tau \propto Q^{-2.5}$, which is close to $\tau \propto Q^{-3/8}$, as suggested by Zilman and Granek.[19,20] However, going into the radial direction, the dynamical behavior cannot be related to any known dynamics. Increasing the side-chain length to $M_n^{side\ chain}$ = 11,500 g/mol enables us to measure mostly the internal side-chain dynamics of the bottlebrush polymer. Hereby, the behavior follows the prediction of Zimm dynamics as well as Zilman and Granek with $\tau \propto Q^{-2.8}$, compatible with the solution condition. In this structural feature, we have small geometrical confinement, which can be seen as constraints arising from the neighbored side chains or fully relaxed dynamics. Combining both samples leads to three consecutive relaxation regimes for bottlebrush polymers in solution, along the backbone in the elongated region, radial along the cross section, and the internal relaxation of the side chains with the blob region.

AUTHOR INFORMATION

Corresponding Authors

Karin J. Bichler − *Department of Chemistry, Louisiana State University, Baton Rouge, Louisiana 70803, United States;* orcid.org/0000-0002-8666-1859; Email: kbichler@lsu.edu

Gerald J. Schneider − *Department of Chemistry, Louisiana State University, Baton Rouge, Louisiana 70803, United States; Department of Physics and Astronomy, Louisiana State University, Baton Rouge, Louisiana 70803, United States;* orcid.org/0000-0002-5577-9328; Email: gjschneider@lsu.edu

Authors

Bruno Jakobi − *Department of Chemistry, Louisiana State University, Baton Rouge, Louisiana 70803, United States;* orcid.org/0000-0003-1171-9486

Dirk Honecker − *ISIS Facility, Rutherford Appleton Laboratory, Didcot OX11 0QX, United Kingdom;* orcid.org/0000-0003-0763-982X

Laura R. Stingaciu − *Neutron Scattering Division, Oak Ridge National Laboratory, Oak Ridge, Tennessee 37831, United States;* orcid.org/0000-0003-2696-5233

Thomas K. Weldeghiorghis − *Department of Chemistry, Louisiana State University, Baton Rouge, Louisiana 70803, United States*

James H. P. Collins − *National High Magnetic Field Laboratory and Biology and McKnight Brain Institute, University of Florida, Gainesville, Florida 32610-0015, United States*

Complete contact information is available at: https://pubs.acs.org/10.1021/acs.macromol.2c01177

Notes

The authors declare no competing financial interest.

ACKNOWLEDGMENTS

The authors acknowledge funding by the U.S. Department of Energy under Grant number DE-SC0019050. This research used resources at the Spallation Neutron Source, a DOE Office of Science User Facility operated by the Oak Ridge National Laboratory. Experiments at the ISIS Pulsed Neutron and Muon Source were supported by a beamtime allocation from the Science and Technology Facilities' Council (10.5286/ISIS.E.RB1920275). A portion of this work was performed in the McKnight Brain Institute at the National High Magnetic Field Laboratory's Advanced Magnetic Resonance Imaging and Spectroscopy (AMRIS) Facility, which was supported by National Science Foundation Cooperative Agreement No. DMR-1644779 and the State of Florida.

REFERENCES

(1) Bichler, K. J.; Jakobi, B.; Huber, S. O.; Gilbert, E. P.; Schneider, G. J. Structural Analysis of Ultrasoft PDMS-g-PDMS Shell -Only Particles. *Macromolecules* **2020**, *53*, 78−89.

(2) Jakobi, B.; Bichler, K. J.; Sokolova, A.; Schneider, G. J. Dynamics of PDMS-g-PDMS Bottlebrush Polymers by Broadband Dielectric Spectroscopy. *Macromolecules* **2020**, *53*, 8450−8458.

(3) Haugan, I. N.; Maher, M. J.; Chang, A. B.; Lin, T.-P.; Grubbs, R. H.; Hillmyer, M. A.; Bates, F. S. Consequences of Grafting Density on the Linear Viscoelastic Behavior of Graft Polymers. *ACS Macro Lett.* **2018**, *7*, 525−530.

(4) Dutta, S.; Wade, M. A.; Walsh, D. J.; Guironnet, D.; Rogers, S. A.; Sing, C. E. Dilute Solution Structure of Bottlebrush Polymers. *Soft Matter* **2019**, *15*, 2928−2941.

(5) Li, Z.; Tang, M.; Liang, S.; Zhang, M.; Biesold, G. M.; He, Y.; Hao, S.-M.; Choi, W.; Liu, Y.; Peng, J.; Lin, Z. Bottlebrush polymers: From controlled synthesis, self-assembly, properties to applications. *Prog. Polym. Sci.* **2021**, *116*, No. 101387.
(6) Zhao, B. Shape-Changing Bottlebrush Polymers. *J. Phys. Chem. B* **2021**, *125*, 6373−6389.
(7) Pesek, S. L.; Li, X.; Hammouda, B.; Hong, K.; Verduzco, R. Small-Angle Neutron Scattering Analysis of Bottlebrush Polymers Prepared via Grafting-Through Polymerization. *Macromolecules* **2013**, *46*, 6998−7005.
(8) Pesek, S. L.; Xiang, Q.; Hammouda, B.; Verduzco, R. Small-Angle Neutron Scattering Analysis of Bottlebrush Backbone and Side Chain Flexibility. *J. Polym. Sci., Part B: Polym. Phys.* **2017**, *55*, 104−111.
(9) Dutta, S.; Pan, T.; Sing, C. E. Bridging Simulation Length Scales of Bottlebrush Polymers Using a Wormlike Cylinder Model. *Macromolecules* **2019**, *52*, 4858−4874.
(10) Theodorakis, P. E.; Hsu, H.-P.; Paul, W.; Binder, K. Computer simulation of bottle-brush polymers with flexible backbone: Good solvent versus theta solvent conditions. *J. Chem. Phys.* **2011**, *135*, No. 164903.
(11) Xiao, L.; Li, J.; Peng, G.; Huang, G. The effect of grafting density and side chain length on the conformation of PEG grafted bottlebrush polymers. *React. Funct. Polym.* **2020**, *156*, No. 104736.
(12) Henn, D. M.; Holmes, J. A.; Kent, E. W.; Zhao, B. Worm-to-Sphere Shape Transition of Thermoresponsive Linear Molecular Bottlebrushes in Moderately Concentrated Aqueous Solution. *J. Phys. Chem. B* **2018**, *122*, 7015−7025.
(13) Peterson, G. I.; Noh, J.; Ha, M. Y.; Yang, S.; Lee, W. B.; Choi, T.-L. Influence of Grafting Density on Ultrasound-Induced Backbone and Arm Scission of Graft Copolymers. *Macromolecules* **2021**, *54*, 4219−4226.
(14) Grigoriadis, C.; Nese, A.; Matyjaszewski, K.; Pakula, T.; Butt, H.-J.; Floudas, G. Dynamic Homogeneity by Architectural Design − Bottlebrush Polymers. *Macromol. Chem. Phys.* **2012**, *213*, 1311−1320.
(15) Bichler, K. J.; Jakobi, B.; Schneider, G. J. Dynamical Comparison of Different Polymer Architectures-Bottlebrush vs Linear Polymer. *Macromolecules* **2021**, *54*, 1829−1837.
(16) Hu, M.; Xia, Y.; McKenna, G. B.; Kornfield, J. A.; Grubbs, R. H. Linear Rheological Response of a Series of Densely Branched Brush Polymers. *Macromolecules* **2011**, *44*, 6935−6943.
(17) Bichler, K. J.; Jakobi, B.; Sakai, V. G.; Klapproth, A.; Mole, R. A.; Schneider, G. J. Short-Time Dynamics of PDMS-g-PDMS Bottlebrush Polymer Melts Investigated by Quasi-Elastic Neutron Scattering. *Macromolecules* **2020**, *53*, 9553−9562.
(18) Iwawaki, H.; Urakawa, O.; Inoue, T.; Nakamura, Y.; Matsumiya, Y.; Watanabe, H. Rheo-Optical and Dielectric Study on Dynamics of Bottlebrush-like Polymacromonomer Consisting of a Polyisoprene Main Chain and Polystyrene Side Chains. *Macromolecules* **2020**, *53*, 7096−7106.
(19) Nettesheim, F.; Wagner, N. J. Fast Dynamics of Wormlike Micellar Solutions. *Langmuir* **2007**, *23*, 5267−5269.
(20) Komura, S.; Takeda, T.; Seto, H.; Nagao, M.Dynamical Fluctuation of Cylindrical Micelles and Membranes in Binary and Ternary Amphiphilic Microemulsion Systems. In *Neutron Spin Echo Spectroscopy*; Springer: Berlin Heidelberg, 2002; pp 302−311.
(21) Richter, D.; Hayter, J.; Mezei, F.; Ewen, B. Dynamical scaling in polymer solutions investigated by the neutron spin-echo technique. *Phys. Rev. Lett.* **1978**, *41*, No. 1484.
(22) Ewen, B.; Richter, D.; Farago, B.; Stühn, B. Neutron spin echo investigations on the segmental dynamics in semidilute polymer solutions under Θ-and good solvent conditions. *J. Non-Cryst. Solids* **1994**, *172*, 1023−1027.
(23) Zilman, A. G.; Granek, R. Undulations and Dynamic Structure Factor of Membranes. *Phys. Rev. Lett.* **1996**, *77*, 4788−4791.
(24) Grillo, I.Small-Angle Neutron Scattering and Applications in Soft Condensed Matter. In *Soft Matter Characterization*; Springer, 2008; pp 723−782.
(25) Higgins, J. S.; Benoit, H. C.; Benoît, H.*Polymers and Neutron Scattering*; Clarendon Press, 1996.
(26) Richter, D.; Monkenbusch, M.; Arbe, A.; Colmenero, J.*Neutron Spin Echo in Polymer Systems*; Springer-Verlag Berlin Heidelberg: Berlin, Heidelberg, 2005; pp 1−221.
(27) Richter, D.; Monkenbusch, M.; Allgeier, J.; Arbe, A.; Colmenero, J.; Farago, B.; Cheol Bae, Y.; Faust, R. From Rouse dynamics to local relaxation: A neutron spin echo study on polyisobutylene melts. *J. Chem. Phys.* **1999**, *111*, 6107−6120.
(28) Richter, D.; Farago, B.; Fetters, L.; Huang, J.; Ewen, B. On the relation between structure and dynamics of star polymers in dilute solution. *Macromolecules* **1990**, *23*, 1845−1856.
(29) Rathgeber, S.; Monkenbusch, M.; Kreitschmann, M.; Urban, V.; Brulet, A. Dynamics of star-burst dendrimers in solution in relation to their structural properties. *J. Chem. Phys.* **2002**, *117*, 4047−4062.
(30) Ohl, M.; Monkenbusch, M.; Arend, N.; Kozielewski, T.; Vehres, G.; Tiemann, C.; Butzek, M.; Soltner, H.; Giesen, U.; Achten, R.; Stelzer, H.; Lindenau, B.; Budwig, A.; Kleines, H.; Drochner, M.; Kaemmerling, P.; Wagener, M.; Möller, R.; Iverson, E. B.; Sharp, M.; Richter, D. The spin-echo spectrometer at the Spallation Neutron Source (SNS). *Nucl. Instrum. Methods Phys. Res., Sect. A* **2012**, *696*, 85−99.
(31) Malo de Molina, P.; Alegría, A.; Allgaier, J.; Kruteva, M.; Hoffmann, I.; Prévost, S.; Monkenbusch, M.; Richter, D.; Arbe, A.; Colmenero, J. Tube Dilation in Isofrictional Polymer Blends Based on Polyisoprene with Different Topologies: Combination of Dielectric and Rheological Spectroscopy, Pulsed-Field-Gradient NMR, and Neutron Spin Echo (NSE) Techniques. *Macromolecules* **2020**, *53*, 5919−5936.
(32) Pagès, G.; Gilard, V.; Martino, R.; Malet-Martino, M. Pulsed-field gradient nuclear magnetic resonance measurements (PFG NMR) for diffusion ordered spectroscopy (DOSY) mapping. *Analyst* **2017**, *142*, 3771−3796.
(33) Momot, K. I.; Kuchel, P. W. Convection-compensating PGSE experiment incorporating excitation-sculpting water suppression (CONVEX). *J. Magn. Reson.* **2004**, *169*, 92−101.
(34) Rathgeber, S.; Pakula, T.; Wilk, A.; Matyjaszewski, K.; Beers, K. L. On the Shape of Bottle-Brush Macromolecules: Systematic Variation of Architectural Parameters. *J. Chem. Phys.* **2005**, *122*, No. 124904.
(35) Mark, J. E.*Polymer Data Handbook*; Oxford University Press, 2009.
(36) Daoud, M.; Cotton, J. P. Star Shaped Polymers: A Model for the Conformation and its Concentration Dependence. *J. Phys.* **1982**, *43*, 531−538.
(37) Gupta, S.; Schneider, G. J. Modeling the dynamics of phospholipids in the fluid phase of liposomes. *Soft Matter* **2020**, *16*, 3245−3256.

https://doi.org/10.1021/acs.macromol.2c01177
Macromolecules 2022, 55, 9810−9819